Title: Hypoxia-inducible factor 1 signaling drives placental aging and can provoke preterm labor

Authors: Erin J. Ciampa[1], Padraich Flahardy[1], Harini Srinivasan[2], Christopher Jacobs[2], Linus Tsai[2], S. Ananth Karumanchi[3], Samir M. Parikh[4]

Affiliations:

[1] Department of Anesthesia, Critical Care, and Pain Medicine, Beth Israel Deaconess Medical Center, Harvard Medical School, Boston MA, USA

[2] Division of Endocrinology, Beth Israel Deaconess Medical Center, Harvard Medical School, Boston MA, USA

[3] Department of Medicine, Cedars-Sinai Medical Center, Los Angeles CA, USA

[4] Division of Nephrology, Departments of Medicine and Pharmacology, University of Texas Southwestern Medical School, Dallas TX, USA

Address correspondence to: Samir Parikh, MD. University of Texas Southwestern Medical Center, Department of Internal Medicine. 5323 Harry Hines Blvd. Dallas, TX 75390-9030. Tel: 214-648-2754. Email: samir.parikh@utsouthwestern.edu.

Abstract:

Most cases of pre-term labor have unknown cause, and the burden of preterm birth is immense. Placental aging has been proposed to promote labor onset, but specific mechanisms remain elusive. We report findings stemming from unbiased transcriptomic analysis of mouse placenta, which revealed that hypoxia-inducible factor 1 (HIF-1) stabilization is a hallmark of advanced gestational timepoints, accompanied by mitochondrial dysregulation and cellular senescence; we detected similar effects in aging human placenta. In parallel in primary mouse trophoblasts and human choriocarcinoma cells, we modeled HIF-1 induction and demonstrated resultant mitochondrial dysfunction and cellular senescence. Transcriptomic analysis revealed that HIF-1 stabilization recapitulated gene signatures observed in aged placenta. Further, conditioned media from trophoblasts following HIF-1 induction promoted contractility in immortalized uterine myocytes, suggesting a mechanism by which the aging placenta may drive the transition from uterine quiescence to contractility at the onset of labor. Finally, pharmacological induction of HIF-1 via intraperitoneal administration of dimethyloxalyl glycine (DMOG) to pregnant mice caused preterm labor. These results provide clear evidence for placental aging in normal pregnancy, and demonstrate how HIF-1 signaling in late gestation may be a causal determinant of the mitochondrial dysfunction and senescence observed within the trophoblast as well as a trigger for uterine contraction.

39 **Introduction:**

40 Preterm birth (birth prior to 37 completed weeks of gestation) is a massive global health
41 burden: it leads all causes of death in neonates and children to the age of 5 worldwide[1], and
42 survivors face a broad array of short- and long-term health challenges[2]. Most preterm births in
43 the United States are due to spontaneous onset of preterm labor, with unknown underlying
44 cause[3]. Preterm labor has proven difficult to treat; there currently exist no highly effective
45 interventions that prevent spontaneous preterm birth (SPTB)[4,5]. The dearth of effective
46 treatments stems from our lack of understanding about the pathways regulating spontaneous
47 onset of labor, both preterm and at term.

48

49 The placenta defines the maternal-fetal interface; it is capable of profoundly influencing both
50 maternal and fetal physiology[6-8], and it is subject to remodeling in response to its local
51 environment[9]. Placental disease is known to contribute to other disorders of pregnancy
52 including preeclampsia[10-12] and intrauterine growth restriction[13,14] and there is increasing
53 interest in its potential role as a driver of preterm labor[15-17].

54

55 Recent studies have found that placentas from pregnancies that resulted in SPTB have unique
56 metabolomic and transcriptomic signatures from term counterparts[18-20]. The reported
57 differences broadly implicate the stress response, inflammation, and various metabolic
58 pathways. It has been challenging to narrow these findings or translate them for mechanistic
59 relevance, given the lack of suitable culture systems that integrate experimental manipulation
60 of placental cells with the uterine myocyte response. Furthermore, interpretation studies

61 profiling human placentas from SPTB is sharply limited by the lack of gestational age-matched
62 controls. Without these, the effects of gestational age cannot be distinguished from factors
63 driving premature labor. The placenta encounters a dynamic local environment across its
64 lifetime and faces evolving needs of the growing fetus, so the context of normal gestational
65 age-related changes is vital for the correct interpretation of molecular characteristics
66 distinguishing a SPTB placenta. Defining the molecular-level changes in the *healthy* placenta as
67 it approaches the end of gestation, and their potential effects on the timing of labor onset
68 would therefore address important knowledge gaps.
69
70 Here we report findings from unbiased transcriptomic analysis of healthy mouse placenta,
71 which highlighted hypoxia-inducible factor 1 (HIF-1) signaling as a hallmark of advanced
72 gestational timepoints, accompanied by mitochondrial dysfunction and cellular senescence. We
73 detected some similar effects in human placentas, then modeled HIF-1 induction with two
74 different stimuli and in two trophoblast cell models, demonstrating that mitochondrial
75 dysfunction and cellular senescence arise secondary to HIF-1 stabilization. Whole transcriptome
76 analysis revealed that upon HIF-1 stabilization, a trophoblast cell line acquires signatures that
77 recapitulate the aged placenta. Finally, we show that conditioned media from these cells is
78 sufficient to potentiate a contractile phenotype in uterine myocytes, implicating a mechanism
79 by which the aging placenta may help drive the transition from uterine quiescence to
80 contractility at the onset of labor. This mechanism is further reinforced by an *in vivo* model in
81 which administration of the prolyl hydroxylase inhibitor dimethyloxalyl glycine (DMOG) to

82 pregnant mice induces HIF-1 signaling in the placenta and causes SPTB.

83

84 **Results**

85 To illuminate gestational age-dependent transcriptional changes in across a healthy pregnancy,
86 we collected whole mouse placentas at 48h intervals spanning embryonic day 13.5 to 17.5
87 (e13.5-e17.5) and quantified mRNA and protein targets that emerged from network analysis of
88 an independently published microarray dataset from healthy mouse pregnancies. Upon
89 searching Gene Expression Omnibus (GEO)[21] datasets for "placenta AND transcriptome", we
90 were surprised that among 326 results, only nine included data from normal placenta across a
91 series of gestational timepoints extending to late pregnancy[22-28] (**Figure 1**). We applied
92 weighted gene correlation network analysis (WGCNA) to a microarray study of mouse
93 placenta[22] (GEO accession GSE11224) spanning e8.5 to postnatal day 0 (p0) to assess the mRNA
94 signature of the aging mouse placenta, using the dataset with the best temporal resolution
95 across gestation. Distinct clusters emerged, each reflecting a group of genes whose expression
96 changes across timepoints in a unified way (**Figure 2A;** accompanying statistics available at
97 Mendeley Data, doi: 10.17632/g6vrw9jjn4.1). Genes in the 'blue' cluster showed increasingly
98 positive correlation with advancing gestational timepoints; KEGG functional pathways
99 significantly overrepresented among these genes include HIF1 signaling, AMPK signaling, and
100 cellular senescence. Genes in the 'turquoise' cluster showed increasingly negative correlation to
101 advancing timepoints; KEGG functional pathways significantly overrepresented among these
102 genes include the citric acid cycle, mitochondrial complex I biogenesis, and the mitotic cell
103 cycle.

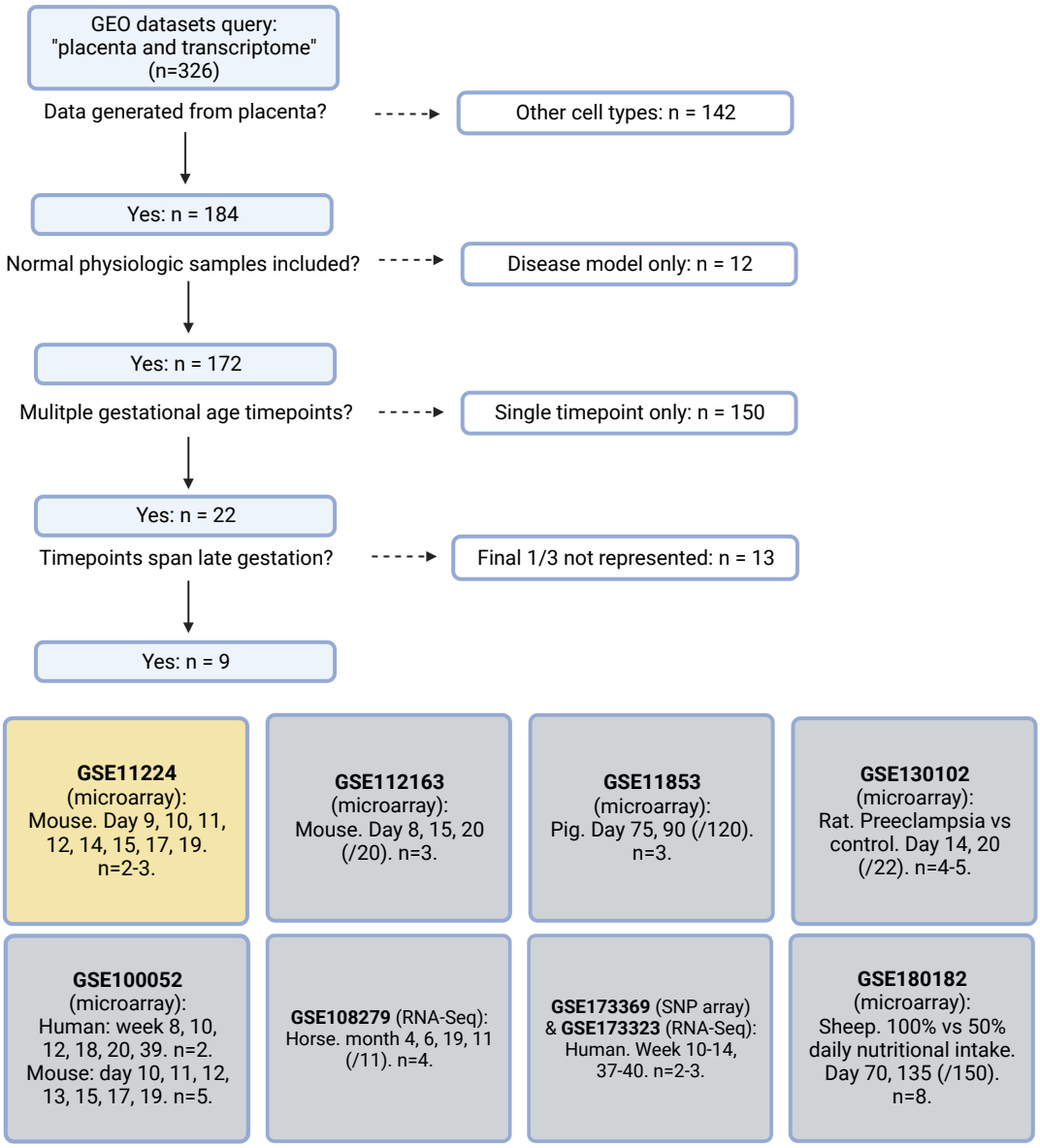

Figure 1. Systematic search flow for placental transcriptomics datasets. 326 GEO datasets were identified by the search terms "placenta" and "transcriptome"; nine met criteria for containing placental transcriptomic data representing normal physiology at a range of gestational timepoints spanning through the final 1/3 of pregnancy. Dataset selected for further analysis in yellow.

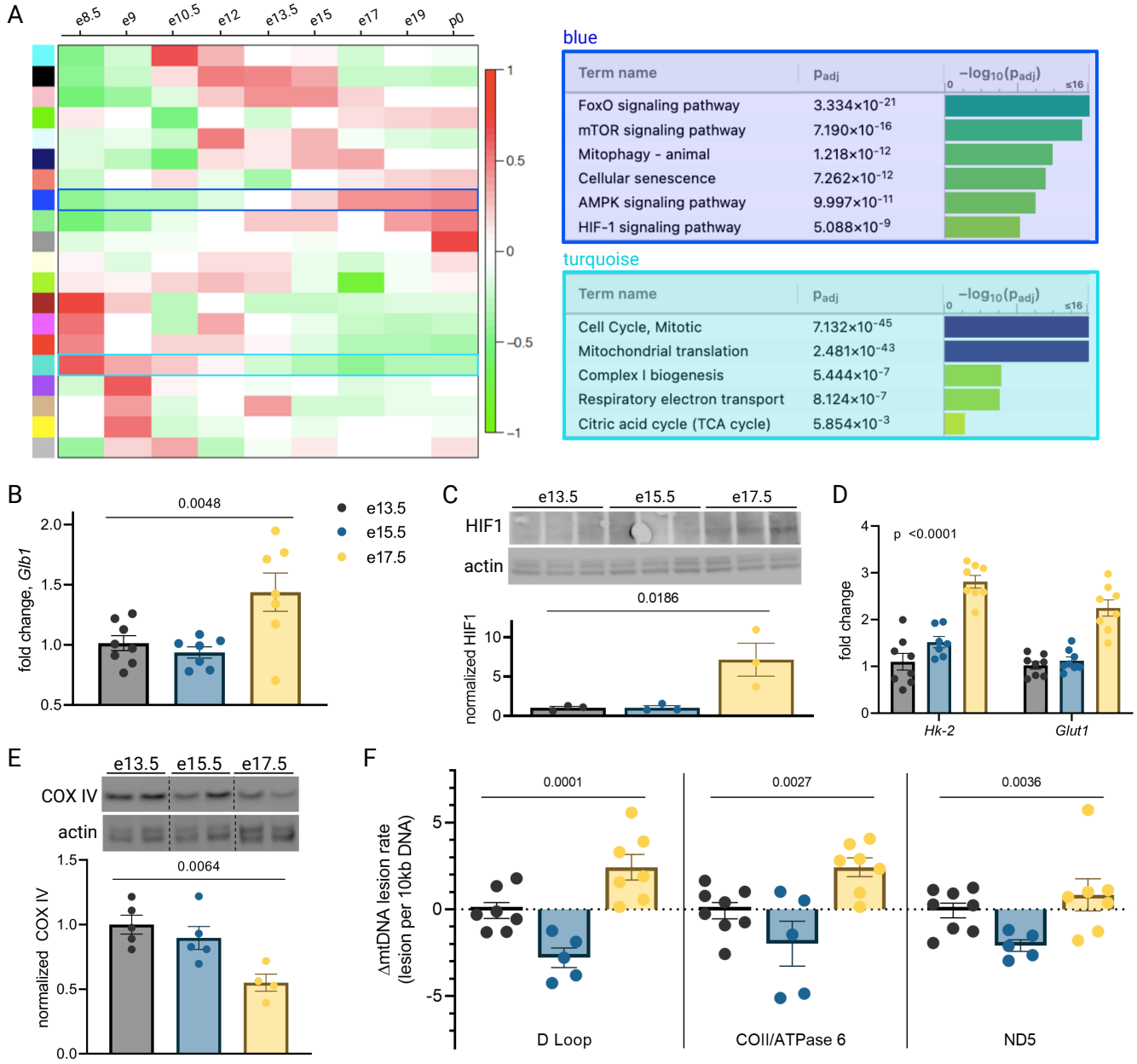

Figure 2. Mouse placental aging is characterized by cellular senescence, HIF-1 signaling, and mitochondrial dysregulation. WGCNA yielded 20 gene clusters. Functional pathways overrepresented in clusters found to increase (blue) and decrease (turquoise) across gestation highlight enhanced cellular senescence, increased HIF-1 signaling, and decreased mitochondrial synthesis and respiration late in pregnancy (A). Expression of senescence marker *Glb1* peaks at e17.5 (B; one-way ANOVA p=0.0048). HIF-1 protein abundance is higher at e17.5 versus e13.5 and e15.5 (C; one-way ANOVA p=0.019), as is expression of HIF-1 targets *Hk2* and *Glut1* (D; two-way ANOVA p<0.0001 for gestational age factor). (See Figure 2 - Supplement 1 for analysis of gene expression changes across timepoints by placental sex.) Mitochondrial abundance, reflected by COX IV protein, decreases with gestational age (E, one-way ANOVA p=0.0064), and mitochondrial DNA lesion rate peaks at e17.5 in the regions of the D-loop (one-way ANOVA p=0.0001), COII/ATPase6 (p=0.0027), and ND5 (p=0.036) (F). B-F, Each data point represents a biological replicate (eg. RNA, protein, or DNA extracted from an individual placenta, in turn collected from one of 2-4 pregnant dams per group). See Figure 2 - Source Data 1 for uncropped, unedited blots.

104

105 To validate the dynamic pathway activity suggested by the WGCNA, we quantified mRNA

106 expression of the senescence marker *Glb1*[29] in our mouse placentas, which mirrored the

107 WGCNA finding that cellular senescence in the placenta peaks in the final days of gestation

108 (**Figure 2B**). HIF-1 protein abundance was found to peak at e17.5 (**Figure 2C**) and HIF-1 targets

109 *Hk2* and *Glut1* likewise confirmed increasing HIF-1 activation with advancing gestational age

110 through e17.5 (**Figure 2D**). Of note, a modest but significant fetal sex-dependent difference in

111 HIF-1 target expression (but not *Glb1*) was also observed across timepoints (**Figure 2 -**

112 **Supplement 1**). To assess changes in mitochondrial abundance across gestation, we measured

113 COX IV protein expression and found it declined progressively across mouse gestation (**Figure**

114 **2E**) as predicted by the WGCNA.

115

116 Having observed a pattern of declining mitochondrial abundance in the placenta with advancing

117 gestational age, we next investigated the mitochondrial DNA (mtDNA) lesion rate. The

118 mitochondrial genome is particularly vulnerable to reactive oxygen species (ROS) insults, and

119 mtDNA damage participates in a vicious cycle with mitochondrial dysfunction and further ROS

120 production; these effects are observed in a number of age-related diseases in various tissues[30]

121 and may drive age-associated loss of function[31]. We employed a semi-long run real-time qPCR

122 approach[32] to quantify relative mtDNA lesion rates in mouse placentas, normalized to e13.5.

123 There was a measurable increase in the mtDNA lesion rate in the D-loop and COII/ATPase 6

124 regions of the mitochondrial genome at e17.5 (**Figure 2F**). Together, these results reflect a

125 series of coordinated changes as gestation progresses —namely HIF-1 signaling induction,

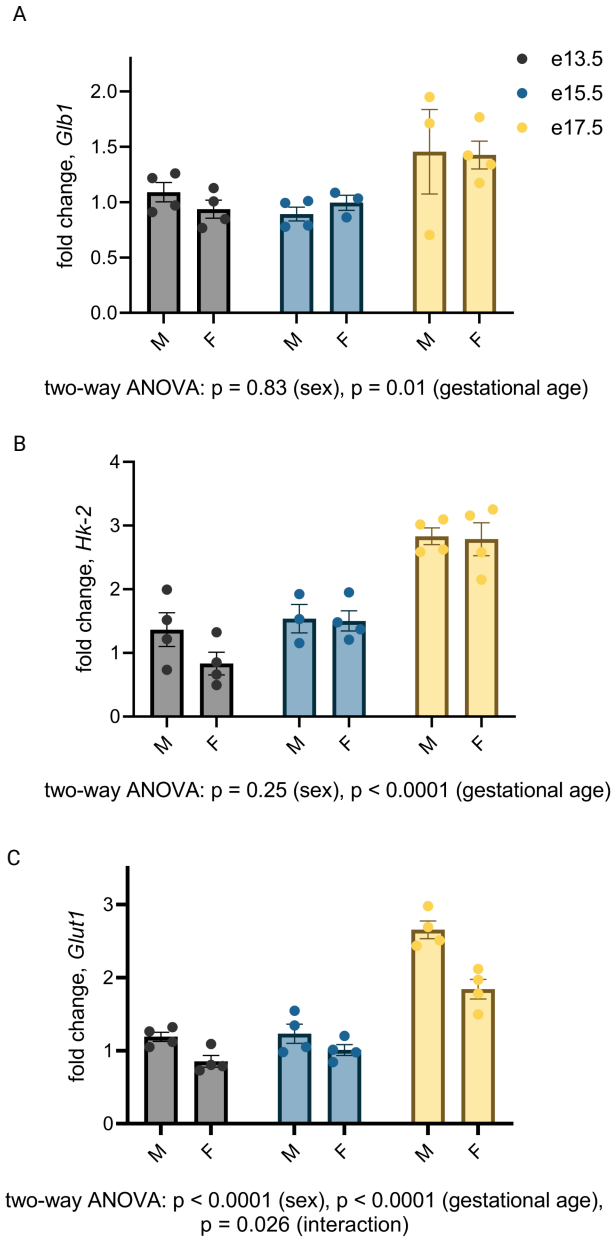

Figure 2 - Supplement 1. Gestational age-dependent variability in expression of Hif-1 target *Glut1*, but not *Hk2*, is affected by placental sex. Subgroup analysis did not reveal sex-dependent expression changes in *Glb1* (A) or *Hk2* (B), but did demonstrate consistently higher *Glut1* expression in male placentas at all gestational ages and an interaction between the effects of sex and gestational age on *Glut1* expression (C; two-way ANOVA p<0.0001 for sex, p<0.0001 for gestational age, and p=0.028 for interaction). Each data point represents a biological replicate (RNA isolated from an individual placenta, collected from one of 2-4 dams per group).

126 decreasing mitochondrial abundance, accumulating ROS stress, and escalating cellular
127 senescence — confirming the patterns we discovered through reanalysis of published
128 transcriptomic data.
129
130 We next probed human placentas for the same gestational age-dependent changes. Studying
131 normal human placenta at a range of gestational ages beyond the second trimester is
132 challenging, as placental sampling is usually only possible after delivery, and most deliveries
133 associated with healthy pregnancies occur at term. We therefore sought to capitalize on rare
134 exceptions such as cases of placenta previa, vasa previa, or uterine dehiscence, where
135 iatrogenic preterm delivery is indicated for reasons unrelated to placental health. With an
136 objective to compare term versus preterm placentas, yet minimize confounding factors that
137 accompany labor and disease states that could be expected to affect placental health, we
138 designed a case-control study using the following exclusion criteria: onset of labor prior to
139 delivery (spontaneous or induced); maternal history of hypertension, asthma, diabetes, or
140 autoimmune disease; pregnancy complicated by gestational hypertension, gestational diabetes,
141 preeclampsia, multiples, fetal anomalies, placenta accreta spectrum disorder, or smoking
142 during pregnancy.
143
144 Placentas from 9 cesarean deliveries occurring before 35 weeks gestation and 11 cesarean
145 deliveries occurring after 39 weeks gestation were studied (**Table 1**). Maternal characteristics
146 including race, nulliparity, and obesity were not statistically different across the early versus
147 late groups; there was a small but statistically significant difference in maternal age at the time

	< 35 weeks	> 39 weeks	p value
	n = 9	n = 11	
Gestational age at delivery (weeks)	34.0 ± 0.3	39.5 ± 0.1	< 0.0001
Maternal age (years)	31.9 ± 0.9	36.2 ± 1.0	0.008
Maternal BMI > 40	1 (11)	0 (0)	0.26
Maternal race			
White	7 (78)	9 (82)	0.13
Black	2 (22)	0 (0)	
Asian	0 (0)	2 (18)	
Primiparous	4 (44)	4 (36)	0.71
Female neonate	5 (55)	8 (73)	0.42
Indication for delivery	Placenta previa (3)	Scheduled repeat (7)	
	Vasa previa (4)	Breech presentation (3)	
	Thinned lower uterine segment (2)	Elective (1)	

Table 1. Maternal and fetal characteristics. Data summarized by mean ± SEM or n (%). p-values calculated via t-test (continuous variables) or Chi-square contingency table (categorical variables).

148 of delivery (31.9 ± 0.9 years versus 36.2 ± 1.0 for early gestation versus late, p = 0.008). The
149 distribution of fetal sex was not different among groups.
150
151 We found a trend toward increased expression of *GLB1* and HIF-1 targets *HK-2* and *GLUT1* in
152 the > 39-week cohort (**Figure 3A**), consistent with the gestational age-dependent effect seen in
153 mouse placenta. We also examined mitochondrial abundance in the two groups and found that
154 mitochondrial RNA transcripts *ATP6* and *COX2* were significantly decreased (**Figure 3B**) and COX
155 IV protein abundance was lower at the later timepoint (**Figure 3C**), mirroring the mouse
156 findings. Of note, power calculation to reject the null hypothesis for difference between means
157 for some of these measurements (with α=0.05 and β=0.2) suggests a sample size of greater
158 than 35 per group is required, assuming a similar effect size as seen in mouse data (eg.
159 expecting *GLB1* fold change difference of 40% across groups), and greater variability than seen
160 for mouse data (eg. expected standard deviation of *GLB1* fold change equal to 0.6, versus 0.3 in
161 mice). Practical constraints, especially given our strict exclusion criteria, make a study of this
162 size unfeasible; nonetheless, we have included analysis of 20 human placentas here in
163 recognition of the vital importance of translating mouse findings to human biology, even
164 preliminarily. The data should be interpreted in the context of these statistical realities.
165
166 The co-appearance of cellular senescence, HIF-1 signaling, and mitochondrial dysregulation in
167 the placenta as it approaches the end of gestation led us to hypothesize that in aging placental
168 cells, HIF-1 induction could be upstream of mitochondrial dysregulation and cellular
169 senescence, as is seen in other systems in emerging aging research[33-35]. To test this hypothesis,

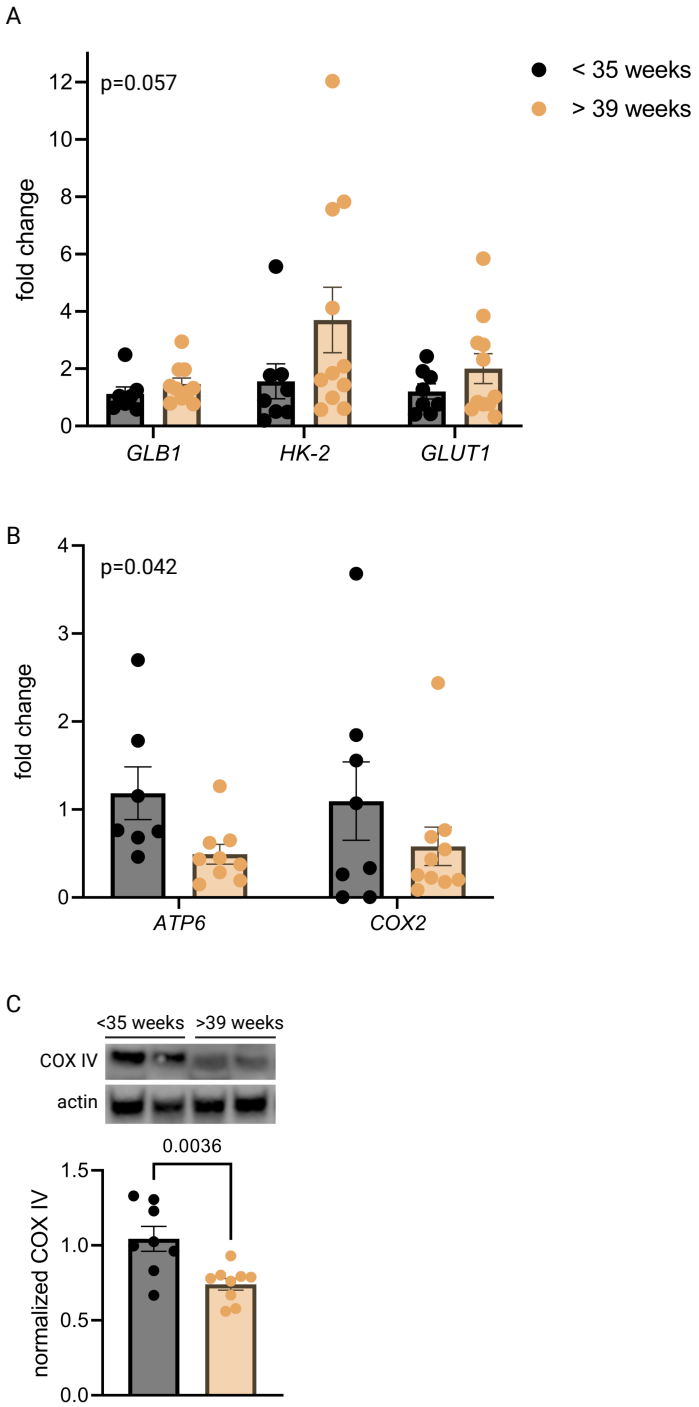

Figure 3. Senescence, HIF-1 signaling, and decreased mitochondrial abundance characterize late-gestation human placenta. Expression of senescence marker *GLB1* and HIF-1 targets *HK-2* and *GLUT1* trends higher in placentas from > 39-week cohort vs < 35-week cohort (A; 2-way ANOVA gestational age factor p=0.057). Mitochondrial abundance, reflected by mitochondrial genes *ATP6* and *COX2* (B; two-way ANOVA gestational age factor p=0.042) and COX IV protein (C; p=0.0036) decreases with advancing gestational age. Each data point represents a biological replicate (RNA or protein isolated from an individual placenta). See Figure 3 - Source Data 1 for uncropped, unedited blots.

170 we established a pharmacological model of HIF-1 induction in primary mouse trophoblasts
171 using cobalt chloride, a prolyl hydroxylase inhibitor that stabilizes HIF-1α[36,37] and has been
172 widely used to model hypoxia. After six hours of $CoCl_2$ exposure, we confirmed HIF-1 protein
173 accumulation in cultured trophoblasts (**Figure 4A**). After 48 hours of $CoCl_2$ exposure, mouse
174 trophoblasts exhibit decreased mitochondrial abundance, by *Cox2* expression (**Figure 4B**) and
175 Cox IV protein abundance (**Figure 4C**), and an increase in senescence-associated beta
176 galactosidase (SA-βGal), encoded by *Glb1* (**Figure 4D**) and detected as a blue stain in an X-gal
177 assay for senescence (**Figure 4E**). These findings suggest that HIF-1 stabilization induces
178 subsequent mitochondrial dysfunction and senescence in trophoblasts.
179
180 Primary trophoblasts undergo spontaneous syncytialization in culture, a phenomenon that
181 limits the duration of study and may also confound the interpretation of experimental changes
182 in key metabolic factors[38]. We therefore also modeled HIF-1 activation in JAR cells, a
183 trophoblast cell line that does not undergo syncytialization[39]. Consistent with our results in
184 primary cells, we found that HIF-1 is stabilized in $CoCl_2$-treated JAR cells (**Figure 5A**), and after 6
185 days of exposure, mitochondrial DNA and protein abundance declined (**Figure 5B-C**). We
186 further defined the time course of mitochondrial downregulation: by 72 hours the effect began
187 to appear (**Figure 5 – Supplement 1**). Furthermore, at the 6-day timepoint we found that $CoCl_2$
188 exposure impairs mitochondrial polarization (**Figure 5D**), and leads to accumulation of
189 mitochondrial reactive oxygen species (**Figure 5E**). Additionally, we observed pronounced signs
190 of cellular senescence: morphological hallmarks (cellular swelling) and β-galactosidase
191 overexpression (**Figure 5F**); growth arrest which persists for days after removal of the HIF-1

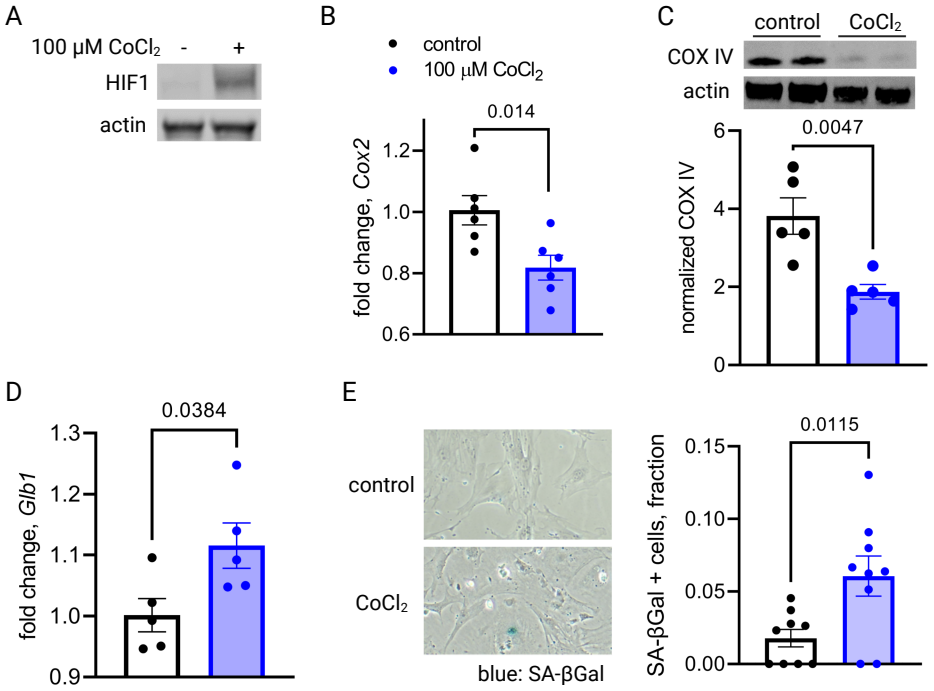

Figure 4. Short-term HIF-1 stabilization in primary mouse trophoblasts leads to decreased mitochondrial abundance and cellular senescence. HIF-1 is detected in cultured trophoblasts exposed to $CoCl_2$ (A). After 48 hours of $CoCl_2$ exposure, trophoblasts exhibit decreased mitochondrial abundance reflected by *Cox2* (B; p=0.014) and COX IV (C; p=0.0047) expression levels. Senescence marker *Glb1* is increased (D; p=0.038) and SA-βGal accumulation is noted by X-gal assay (E; p=0.012). Each data point represents a technical replicate (eg. protein, RNA, or β-Gal measured from an individual well of cells grown in treated or control condition). See Figure 4 - Source Data 1 for uncropped, unedited blots.

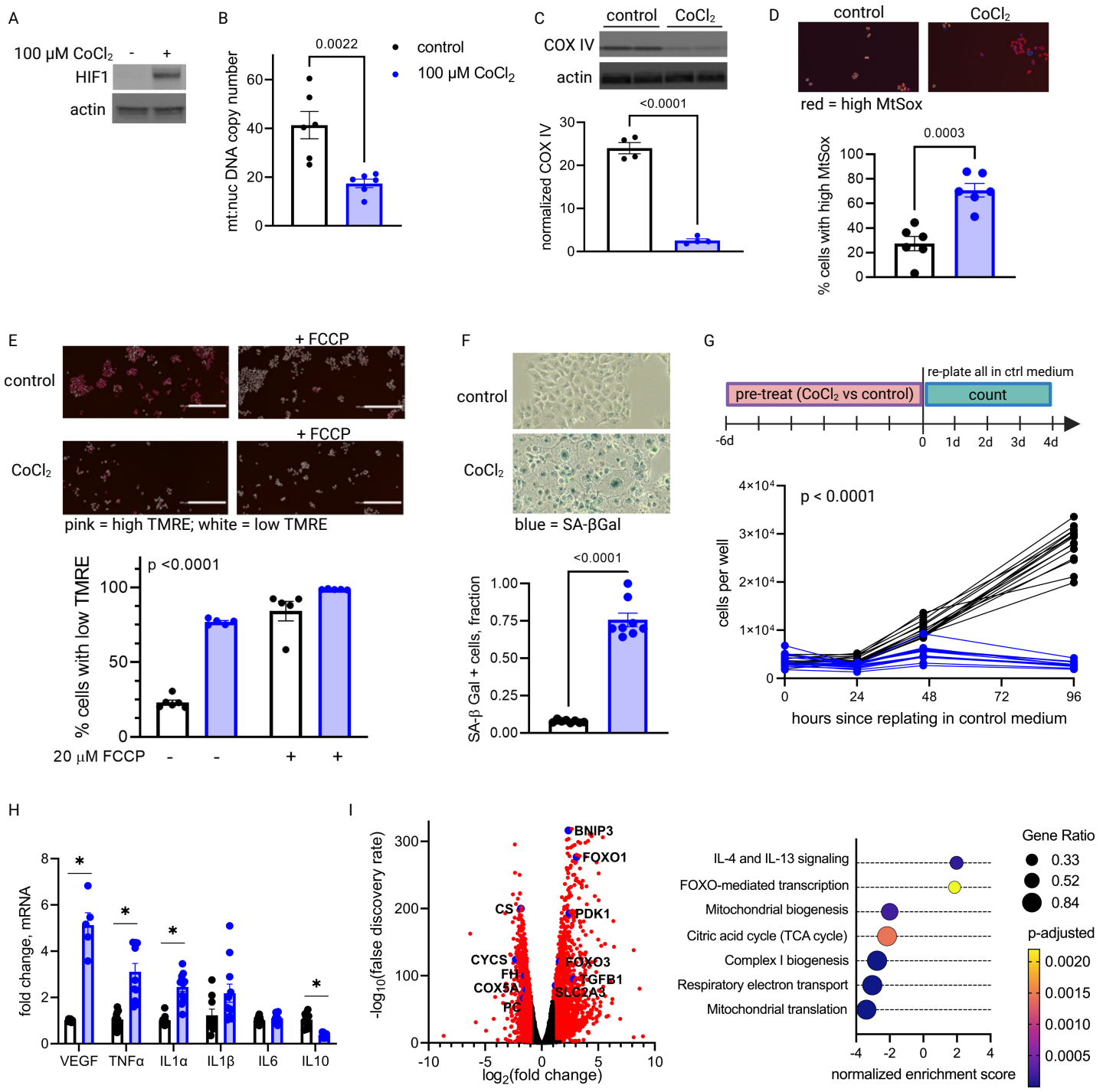

Figure 5. Long-term HIF-1 stabilization in JAR cells leads to mitochondrial dysfunction, cellular senescence, and metabolic reprogramming. JAR cell exposure to $CoCl_2$ stabilizes HIF1 (A). After 6 days, mitochondrial abundance is decreased as reflected by a drop in the mitochondrial:nuclear DNA copy number (B) and a decrease in COX IV protein (C). (See Figure 5 - Supplement 1 for timecourse of COX IV downregulation.) Cells also exhibit augmented signs of mitochondrial dysfunction, including MtSox (D) and TMRE staining (E; two-way ANOVA $CoCl_2$ factor p<0.0001). SA-βGal staining reflects a high proportion of senescent cells (F) and growth arrest is confirmed by cell counting following a 6-day pre-treatment with $CoCl_2$ (G; two-way ANOVA p<0.0001 for interaction of $CoCl_2$ factor with time). (See Figure 5 - Supplement 2 for assessment of cell death by propidium iodide staining.) SASP candidates VEGF, TNFα, IL-1α, and IL10 are dysregulated after $CoCl_2$ exposure (H; *, adjusted p<0.01). RNA Seq revealed upregulation of 2188 and downregulation of 1389 genes (I; genes with $|\log_2(FC)| > 1$ and -log(FDR)>2 indicated in red) after $CoCl_2$ treatment, with geneset enrichment analysis revealing several pathways significantly dysregulated after $CoCl_2$ treatment recapitulating changes seen in transcriptomic analysis of late versus early gestation mouse placenta. Scale marker = 200 μm. See Figure 5 - Supplement 3 for assessment of effects of HIF-1 stabilization in JAR cells using DMOG. Each data point represents a technical replicate (measurement from an independent well of cells grown in treatment vs control condition). See Figure 5 - Source Data 1 for uncropped, unedited blots.

192 stabilizing compound (**Figure 5G**); and a senescence-associated secretory phenotype (SASP,
193 **Figure 5H**) reflected by increases in expression of VEGF, TNFα and IL-1α and a decrease in the
194 anti-inflammatory cytokine IL-10.
195
196 We conducted additional studies to confirm that cell death was not a primary contributor to
197 the lack of proliferation. Propidium iodide staining with quantitative fluorescence cytometry
198 indicated that $CoCl_2$ treatment only increased cell death by 0-3% (**Figure 5 - Supplement 2**).
199 Importantly, cells remained adherent and continued to acidify culture medium beyond 14 days
200 of $CoCl_2$ exposure, providing confidence that HIF-1 stabilization induces a phenotype
201 characterized by predominantly viable cells that are no longer proliferating, namely cellular
202 senescence. Finally, to assess whether the effects we observed were attributable to HIF-1
203 stabilization and not an off-target effect of $CoCl_2$, we also evaluated an alternative prolyl
204 hydroxylase inhibitor, dimethyloxalylglycine (DMOG)[40], and found similar effects on HIF-1,
205 mitochondrial abundance and cellular senescence (**Figure 5 – Supplement 3**).
206
207 To determine if other features of the aged placenta phenotype were recapitulated in this
208 model, we performed whole transcriptome analysis via RNA-Seq. Differential expression ($\log_2$
209 fold change > 1; FDR < 0.05) was found for 2188 upregulated and 1389 downregulated genes
210 (**Figure 5I**). Gene set enrichment analysis revealed that chemical hypoxia led to upregulation of
211 inflammatory signaling, and downregulation of the TCA cycle, mitochondrial biogenesis, and
212 respiratory electron transport. These data therefore recapitulated metabolic patterns that
213 emerged from time course transcriptomic analysis of intact placentas (Figure 2A).

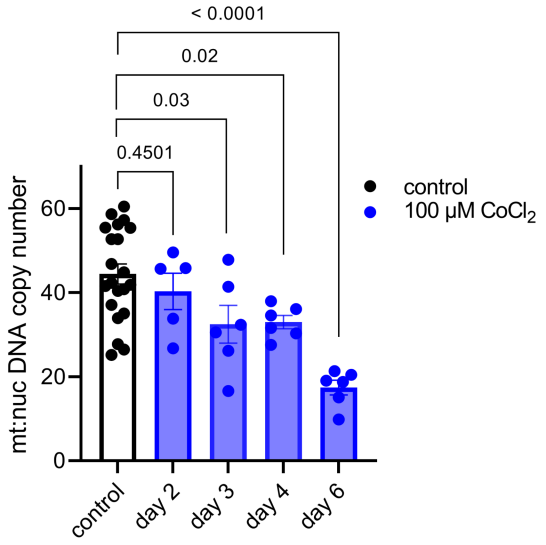

Figure 5 - Supplement 1. The mitochondrial effects of HIF-1 stabilization in JAR cells begin to appear on day 3 following $CoCl_2$ exposure. Each data point represents a technical replicate (independent well of cells grown in control vs treatment condition).

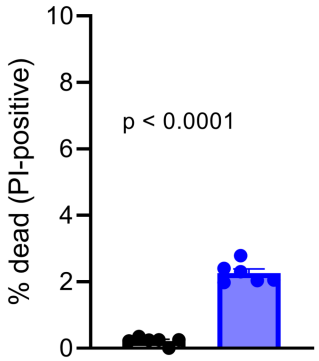

Figure 5 - Supplement 2. Increased number of JAR cells stain with propidium iodide, but the absolute number remains low following 6 days of $CoCl_2$ treatment. Each data point represents a technical replicate (independent well of cells grown in control vs treatment condition).

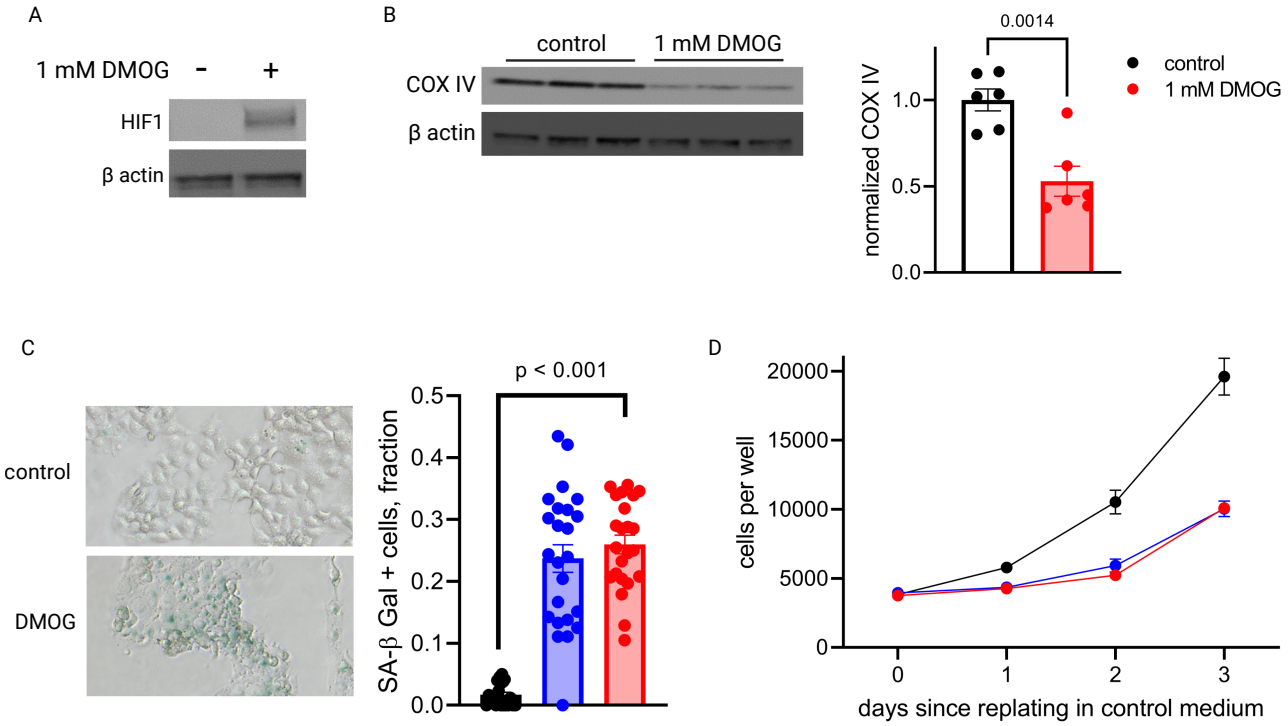

Figure 5 - Supplement 3. DMOG stabilizes HIF-1 in JAR cells (A) and induces similar effects as $CoCl_2$ on COX IV protein (B), SA-βGal expression (C), and cell growth (D) after 4 days. Each data point represents a technical replicate (measurement from an independent well of cells grown in treatment vs control condition). See Figure 5 - Source Data 1 for uncropped, unedited blots.

214

215 The onset of labor is accompanied by a transformation of the uterus from quiescence into a
216 distinct physiologic state in which it generates powerful, coordinated contractions. This
217 phenotypic change is characterized by upregulation of a cadre of contraction associated
218 proteins (CAPs), notably: cyclooxygenase-2 (COX-2, encoded by *PTGS2*), prostaglandin F2α
219 receptor (encoded by *FP*), interleukin-6 (IL-6), and connexin 43 (Cx43, encoded by *GJA1*)
220 Phenotypic switching can be modeled in primary and immortalized uterine myocytes upon
221 stimulation with inflammatory mediators such as IL1β, PGF2α, and thrombin[41-43].

222

223 To test whether primary placental metabolic disruptions could crosstalk with uterine myocytes
224 to trigger the contractile phenotype, we collected conditioned media from our JAR cell model
225 of HIF-1-driven senescence and measured the effect on expression of CAPs in uterine myocytes
226 (hTERT-HM cells). We observed a robust and specific effect: co-stimulation of uterine myocytes
227 with IL-1β plus conditioned media from JAR cells treated with $CoCl_2$ (but not from untreated
228 JAR cells) potentiated the induction of *PTGS2*, *GJA1*, *FP*, and *IL-6* expression (**Figure 6A-D**). We
229 next employed a collagen lattice assay previously described for assessing contractility of
230 myometrial cells *in vitro*[41,44], and demonstrated that myocyte contraction is augmented upon
231 exposure to conditioned media from JAR cells treated with $CoCl_2$ but not from untreated JAR
232 cells (**Figure 6E**). These transcriptional and functional results collectively demonstrate that
233 uterine myocytes are responsive to the secretome of JAR cells driven to senescence via HIF-1
234 induction.

235

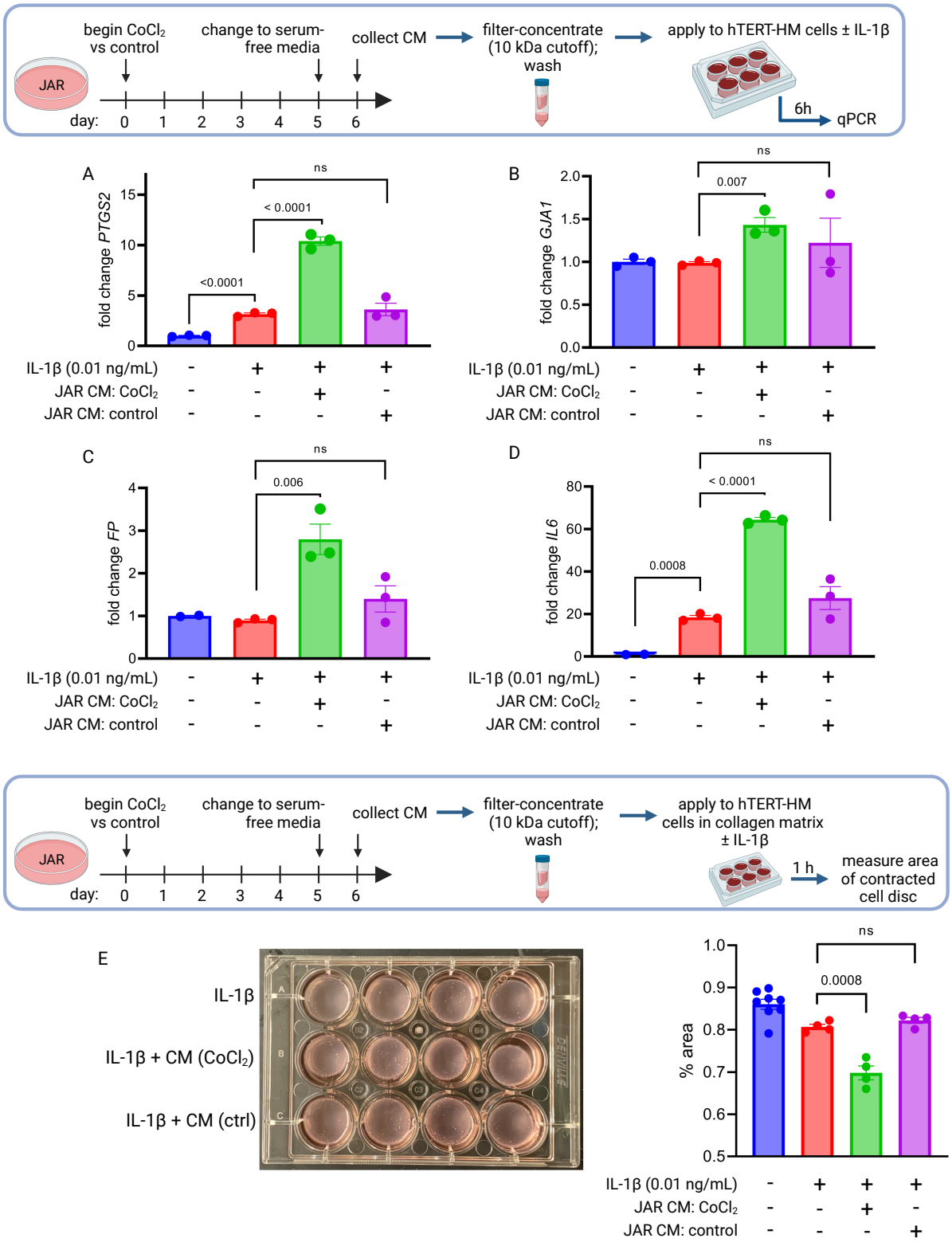

Figure 6. Conditioned media (CM) from JAR cells following HIF-1 stabilization induces expression of contractile-associated proteins and augments contraction in immortalized human uterine myocytes. hTERT-HM expression of *PTGS2* (A), *GJA1* (B), *FP* (C), and *IL6* (D) was induced by CM from JAR cells following $CoCl_2$ treatment (but not in control conditions), similar to (in some cases potentiating) the effect of stimulation of myocytes by exogenous IL-1β. Percent well area occupied by hTERT-HM cells embedded in collagen matrix is significantly smaller after stimulation with IL-1β plus JAR CM from $CoCl_2$ condition, reflecting greater degree of hTERT-HM cellular contraction (E). Each data point represents a technical replicate (measurement from an independent well of cells grown in treatment vs control condition).

236 To test whether HIF-1 induction drives labor onset *in vivo*, we administered DMOG
237 intraperitoneally to pregnant mice on gestational day e16.5. Analysis of placentas recovered 12
238 hours following injection indicated that HIF-1 protein is stabilized in placenta following
239 maternal DMOG injection (**Figure 7A**), and transcription of HIF-1 target genes *Hk-2* and *Glut1*
240 was significantly increased (**Figure 7B**). Following injection of DMOG, gestational length was
241 significantly shortened compared to injection of vehicle alone (**Figure 7C-D**).
242

243 **Discussion**

244 The subject of whether the healthy placenta undergoes aging (with accompanying dysfunction)
245 within its 40-week lifespan has been of great interest and debate for many years. Age-related
246 functional decline is a near-universal phenomenon affecting many tissues, but the underlying
247 biochemical driving factors vary widely depending on the context of cell type and local
248 stressors. Mechanisms well described in other tissues are rooted in genomic instability,
249 mitochondrial dysfunction and oxidative stress, nutrient deprivation and metabolic
250 insufficiency, or loss of proteostasis[45]. While characterization of the placenta as an aging organ
251 appeared in the literature beginning nearly fifty years ago[46,47], a counter-argument has been
252 offered that there is no logical reason for the placenta to undergo accelerated aging relative to
253 the fetus, since both share the same genes and environment[48]. A third viewpoint proposes that
254 aging in the placenta is indicative of a disease state—not normal progression of healthy
255 gestation—one usually reflective of maladaptive responses to oxidative stress[49-53]. Finally,
256 recent reports have noted prominent signs of aging in another fetally derived tissue, the
257 chorioamniotic membranes, in healthy pregnancies[54], and have linked aging of the fetal

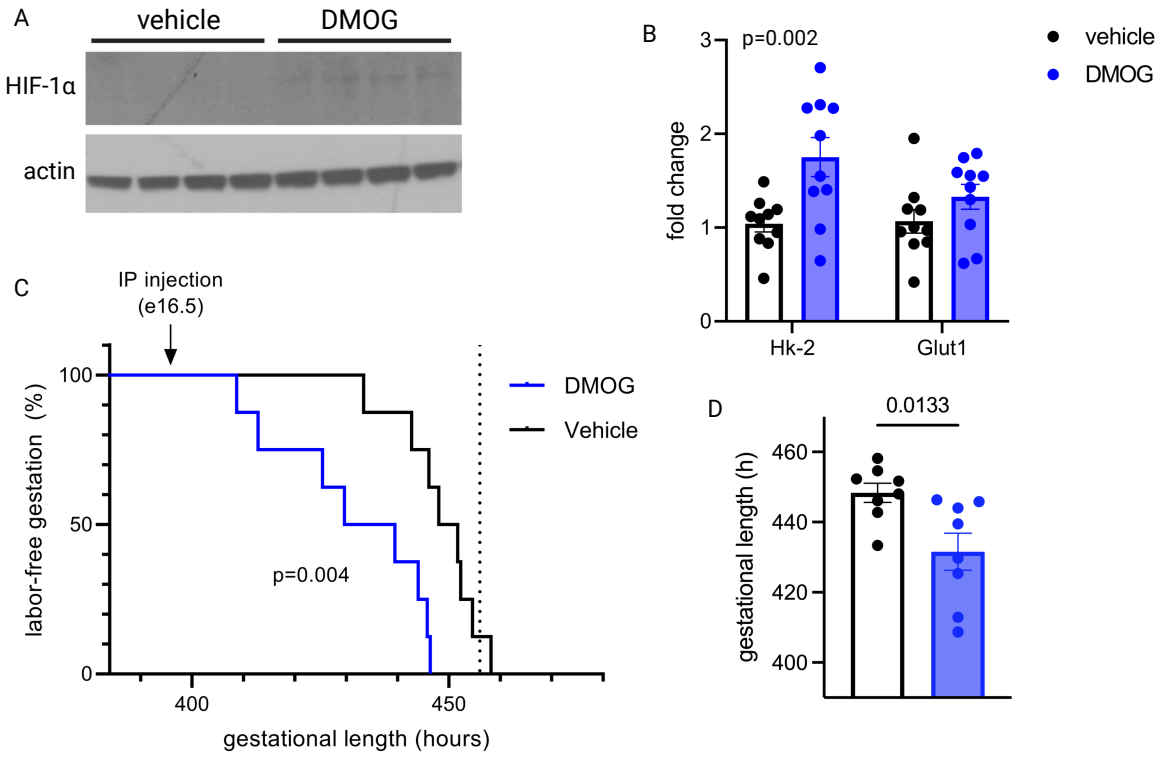

Figure 7. Maternal DMOG injection on e16.5 stabilizes placental HIF-1 and induces preterm labor. HIF-1α protein is detected in placental lysates 12 hours following DMOG injection but not vehicle (A). HIF-1 targets *Hk-2* and *Glut1* are upregulated following DMOG injection (p = 0.002 for DMOG vs vehicle, two-way ANOVA) (B). Gestational length is significantly shortened following DMOG injection versus vehicle (C-D). Each data point represents a biological replicate (in A and B, each measurement from an individual placenta collected from one of 2 pregnant dams). See Figure 7 - Source Data 1 for uncropped, unedited blots.

258 membranes to the onset of labor[55,56]. The results presented here span mouse and human
259 placentas to provide evidence for placental aging in normal pregnancy. Mechanistic dissection
260 of this phenomenon further demonstrates how hypoxia in late gestation may be both a causal
261 determinant of mitochondrial dysfunction and senescence observed within the trophoblast as
262 well as a trigger to induce uterine contraction.
263
264 To our knowledge, this is the first report to propose that placental aging in healthy pregnancy is
265 characterized by induction of HIF-1 signaling, accompanied by downstream effects including
266 mitochondrial dysfunction and cellular senescence. These findings have implications for the role
267 of the placenta in signaling that promotes the onset of labor, particularly given our
268 demonstration that upon HIF-1 stabilization, trophoblasts can induce inflammatory changes in
269 uterine myocytes and potentiate their contractility, and our *in vivo* demonstration that
270 administration of DMOG stabilizes placental HIF-1 and leads to preterm labor in mice.
271 Important next steps prompted by this work include determining the specific components of
272 the secretome of HIF-1-activated trophoblasts which are responsible for inducing myocyte
273 transformation. Additionally, having established that HIF-1 signaling is upstream of
274 mitochondrial dysfunction and cellular senescence in late-gestation trophoblasts in normal
275 pregnancies, future studies can investigate whether factors that modulate this pathway could
276 increase or decrease vulnerability to preterm labor. In studies targeted to uterine decidua, a
277 link between cellular senescence and labor onset has previously been established, with
278 evidence implicating phospho-Akt and mTORC1 signaling upstream of prostaglandin synthesis
279 as a key mechanism in this model[57,58]. It is possible that senescence signaling from the placenta

280 and decidua converge, and labor is provoked upon these convergent endpoint signals
281 surpassing a threshold, regardless of their origin within the gestational compartment.
282
283 Our results suggest that placental HIF-1 becomes stabilized late in gestation, and this could be
284 secondary to the onset of hypoxia sensing as oxygen demand outstrips supply in the
285 fetoplacental unit. However, placental hypoxia has been difficult to examine *in vivo*. Despite
286 evolving approaches for measurement of placental oxygenation, findings have varied widely
287 and adequate spatiotemporal resolution has so far been challenging[59]. However, it is apparent
288 that due to arteriovenous shunting and high metabolic extraction rates, the placenta
289 experiences hypoxia throughout pregnancy with a reported partial pressure of oxygen 30-50
290 mm Hg in the intervillous space, so perhaps a relevant question is what *prevents* HIF-1
291 stabilization and its downstream effects early in gestation. It is possible that the gestational-
292 age-dependent HIF-1 induction we observed reflects not a change in oxygen availability, but
293 rather a change in other HIF-regulatory factors such as nicotinamide adenine dinucleotide
294 (NAD^+) depletion, as has been demonstrated to occur in muscle and is accompanied by
295 metabolic reprogramming and mitochondrial decline[60]. Importantly, replenishment of NAD^+
296 was shown to restore markers of mitochondrial function in these aged cells, suggesting that
297 mitochondrial effects of HIF-1-driven aging are reversible in some systems. Separately, a recent
298 study which compared the miR-nomes of 1st- versus 3rd-trimester human placenta highlighted
299 differential expression of miRNAs with functional links to silencing of hypoxia response and
300 cellular senescence pathways in the first trimester[61]. Future investigations into the impact of
301 placental HIF-1 regulation will require a more precise understanding of placental oxygenation *in*

302 *vivo* and a sophisticated approach to model these factors in placental explants or other cellular
303 systems.
304
305 The shift in metabolic phenotype away from oxidative respiration in late pregnancy as
306 demonstrated by our transcriptomics analysis is consistent with earlier findings from
307 respirometry studies in mouse placenta[62], where rates of oxidative phosphorylation were noted
308 to decline from e14 to e19, particularly in the labyrinthine zone. It is still unclear if this shift
309 reflects changing substrate availability, or oxygen content, or perhaps the metabolic needs of
310 the developing fetus. A better understanding of the dynamic metabolism of the placenta across
311 gestation will be crucial for developing strategies for optimizing placental health, with major
312 implications for both maternal and fetal outcomes. For example, placental metabolomics
313 studies with a gestational time series could help corroborate the metabolic implications
314 interpreted from our transcriptomic data, while single-cell transcriptomics across advancing
315 gestational age in healthy placentas would offer critical cell-type localization of specific
316 metabolic events noted to occur late in pregnancy. Future studies aimed at targeted
317 manipulation of placental metabolism *in vivo*, whether pharmacologically or genetically, are
318 needed to define the physiologic relevance of these findings.
319
320 Our data have implications for other adverse pregnancy outcomes beyond preterm birth,
321 including intrauterine growth restriction and preeclampsia. An important study previously
322 examined mice with placental expression of a constitutively active HIF-1 mutant and found that
323 when induced from the beginning of gestation, placental HIF-1 signaling drives abnormal

324 placentogenesis and impaired spiral artery remodeling, leading to placental hypoperfusion,
325 fetal growth restriction, and a preeclampsia-like clinical syndrome[63]. In the context of these
326 earlier results, our study highlights the critical gestational age-dependence of HIF-1 effects,
327 having demonstrated that in a normally developed mouse placenta, induction of HIF-1 signaling
328 during the final days of gestation leads to labor onset. Timing may be key to understanding how
329 two distinct pregnancy complications – preterm labor and preeclampsia – appear to emerge
330 separately from overlapping pathophysiologic mechanisms[64-68].
331
332 In summary, we report a molecular characterization of placental aging phenomena occurring in
333 normal pregnancies, stemming from induction of HIF-1 signaling and downstream
334 mitochondrial dysfunction and cellular senescence. These findings establish aging in the
335 placenta as a feature of normal gestation; identify HIF-1 signaling as an upstream trigger
336 leading to mitochondrial dysfunction and senescence in the placenta; demonstrate that the
337 secretome of senescent trophoblasts is sufficient to potentiate uterine myocyte transformation
338 and contractility; and establish that HIF-1 induction *in vivo* can induce preterm labor. These
339 findings may have important implications for illuminating the factors that determine gestational
340 length both in health and disease.
341
342 **Data Availability:**
343 Statistics accompanying WGCNA (Figure 2) are accessible through Mendeley Data, doi:
344 10.17632/g6vrw9jjn4.1. (https://data.mendeley.com/datasets/g6vrw9jjn4/1)
345

346 The RNA Seq dataset has been deposited in NCBI's Gene Expression Omnibus[21] and is accessible

347 through GEO Series accession number GSE199278.

348 (https://www.ncbi.nlm.nih.gov/geo/query/acc.cgi?acc=GSE199278)

349 Additional source data (original images for all blots) available in attached files.

350

351 **Methods:**

352 *Mouse placenta collection:* Wild-type C57BL/6 mice (Jackson Laboratory #000664) were fed a

353 chow diet and housed at 20°C in a 12-hour light/12-hour dark cycle. Nulliparous females (< 6

354 months of age) were housed for a single dark cycle (midnight = gestational day 0) with a stud

355 male. On gestational day e13.5-17.5, placentas were isolated via laparotomy from pregnant

356 females anesthetized via surgical-plane isoflurane. Placentas were quartered, immersion-rinsed

357 in dH_2O and blotted dry, then snap frozen in liquid nitrogen and stored at -80°C prior to use.

358

359 *Mouse trophoblast isolation:* Protocol described in full in Pennington *et al*[69]. On gestational day

360 e15.5, placentas were collected via laparotomy from pregnant wild-type C57BL/6 female mice

361 anesthetized with surgical-plane isoflurane. After dissection, placentas were quartered,

362 immersion-rinsed in dH2O, then placed in ice-cold digestion buffer: DMEM plus HEPES 20 mM,

363 collagenase 1mg/mL, and DNase I 4000U/mL. Placentas were digested for 20-40 minutes at

364 37°C with trituration and examined under a microscope until optimal digestion achieved.

365 Digested cells were passed through a 70 micron strainer, washed in DMEM, then separated

366 using a Percoll gradient. Trophoblast fraction was washed once more then plated in complete

367 medium: DMEM with HEPES 20 mM, FBS 10%, and supplemented with sodium pyruvate, pen-
368 strep-glutamine, non-essential amino acids, and gentamicin.
369
370 *Mouse DMOG injection and measurement of gestational length*: On gestational day e16.5, dams
371 received an intraperitoneal injection of DMOG (Selleck Chemicals) 7.5 mg in 0.3 mL sterile
372 saline (approximately 250 mg/kg) versus vehicle alone. Video recordings were used to measure
373 gestational length, defined as interval from midnight of timed mating period until birth of the
374 first pup.
375
376 *Human placental specimens.* Placenta samples were collected at the time of cesarean delivery,
377 within 20 minutes of delivery of the placenta. Placental tissue was sampled from approximately
378 1cm deep to the maternal surface after dissecting away membranes. Cotyledons from all 4
379 quadrants were collected and minced together prior to immersion rinse in dH_2O and storage of
380 separate aliquots by snap freezing versus immersion in RNA Later. All samples were stored at -
381 80°C prior to use.
382
383 *Cell culture.*
384 JAR choriocarcinoma cells (ATCC HTB-144) were grown in RPMI1640 media (4.5 g/L glucose)
385 with 10% FBS. Adherent JAR cells were treated with HIF1-stabilizing agents dissolved in 1X PBS
386 (pH 7.4): cobalt chloride hexahydrate (100 µM $CoCl_2$, Millipore Sigma) and
387 dimethyloxalylglycine, N-(methoxyoxoacetyl)-glycine methyl ester (1 mM DMOG, Millipore

388 Sigma). JAR cells were treated with 100 µM $CoCl_2$ or 1 mM DMOG in culture media as indicated
389 prior to endpoint assays.
390
391 Preparation of conditioned media: On day 5 of JAR cell treatment with $CoCl_2$ (versus control
392 condition), media exchange was performed to apply serum-free media for both conditions. 24
393 hours later, conditioned media samples were collected and applied to 10 kDa molecular weight
394 cutoff filters (Amicon Ultra), with centrifugation for 20 minutes at 4000 x *g*, 4°C. Filters were
395 washed with one volume of hTERT-HM base medium (see below), with repeat centrifugation.
396 Concentrated proteins retained in suspension above the filter were collected and stored at -
397 80°C.
398
399 hTERT-HM cells (generously supplied by Dr. Jennifer Condon, Wayne State) were grown in
400 DMEM/F12 medium (Gibco) with 10% FBS and Antibiotic-Antimycotic (1X, Gibco). Cells were
401 stimulated by addition of recombinant human IL-1 (R&D Systems) and/or filter-concentrated
402 JAR cell conditioned media as indicated, 6 hours prior to collection of cellular RNA.
403
404 *RT – qPCR*. Total RNA was reverse transcribed to cDNA with the Superscript III reverse
405 transcriptase (Invitrogen) system with random hexamer primers (Invitrogen) according to
406 manufacturer's instructions. cDNA was amplified via real-time quantitative PCR with TaqMan
407 Fast Advanced Master Mix (Applied Biosystems) or SYBR Green PCR Master mix (Qiagen) in a
408 QuantStudio 6 Flex Real-Time PCR System (Applied Biosystems). In mouse samples, target gene
409 expression was normalized to endogenous levels of housekeeping gene, β-actin. In human

410 samples, target gene expression was normalized to endogenous levels of housekeeping gene,

411 YWHAZ (TaqMan) or β-actin (SYBR). Mouse and human primers are listed in Table 2.

412

413 *Collagen lattice contraction assay*: As previously described[41,44], hTERT-HM cells were suspended

414 in a collagen gel matrix (Cellmatrix collagen type I-A, Fisher Scientific, prepared with MEM,

415 NaOH and HEPES) then plated in 12-well dishes and grown in hTERT-HM medium. When cells

416 reached approximately 60% confluence, gel matrix was detached from plate and experimental

417 treatments were applied in fresh cell culture medium. After 1 hour incubation, a photograph

418 was taken of each well for measurement of percent well area occupied by collagen disc,

419 reflecting cellular contraction.

420

421 *mtDNA damage assay.* Mitochondrial DNA damage was assayed from total DNA via a semi-long

422 run real-time PCR approach, as described elsewhere[32]. Briefly, separate qPCR reactions were

423 assayed to compare a long versus short amplicon representing each genomic region. A lesion

424 rate per 10 kb of mtDNA was calculated as:

425 lesion rate $= \frac{10000\ (bp)}{size\ of\ long\ fragment\ (bp)} * (1 - FC_{long-short})$,

426 with $FC_{long-short} = 2^{-\Delta\Delta Ct}$ calculated in the usual method.

427

428 *Relative mtDNA copy number.* qPCR assays for nuclear and mitochondrial genes were

429 performed using total DNA as a template. Relative mitochondrial DNA was calculated as:

430 follows:

431 mt:nuc DNA copy number $= 2 * 2^{\Delta Ct}$, where $\Delta Ct = Ct_{nuclear\ gene} - Ct_{mitochondrial\ gene}$.

432

433 *Immunoblots.* Antibodies are listed in Table 3.

434

435 *SA-β-Galactosidase Assay.* Adherent cells were fixed and stained for SA-βGal via a Senescence

436 Detection kit (Abcam, ab65351) per manufacturer's instructions. Representative images were

437 used to calculate the fraction of SA-β-Gal-positive cells, scored by an observer blinded to

438 treatment condition.

439

440 *Live cell staining.* Adherent cells were stained using the TMRE-Mitochondrial Membrane

441 Potential Assay Kit (Abcam, ab113852) per manufacturer's instructions. Select wells were

442 pretreated with 20 µM FCCP, a decoupling agent, as a positive control for 20 minutes before

443 TMRE and Hoechst counterstain was applied. Live JAR cells were analyzed by the Celigo Image

444 Cytometer (Nexcelom BioScience) for fluorescence quantification and gating. Adherent live JAR

445 cells were stained with MitoSOX™ Red Mitochondrial Superoxide Indicator kit (Invitrogen) and

446 analyzed using the cytometer in a similar manner.

447

448 *Cell counting.* JAR cells were cultured for 6 days ± cobalt chloride exposure prior to cell

449 counting. On day 6, cells from each condition were replated in a 96-well plate in $CoCl_2$-free

450 media at a density of 5×10^3 cells per well. Celigo Image Cytometer was used for automated cell

451 counting (total cells per well) at 24-hour intervals.

452

Table 2. Primers

Mouse

Target	Sequence	Platform
GLB1	Mm00515342_m1	TaqMan
HK-2	Mm00443385_m1	TaqMan
GLUT1	Mm00441473_m1	TaqMan
D loop (long, 801 bp amplicon)	F: CGTACATTAAACTATTTTCCCCAAG R: GAGTTTTGGTTCACGGAACAT	SYBR
COII/ATPase 6 (long, 855 bp amplicon)	F: TTGGTCTACAAGACGCCACA R: ATTTTGGTGAAGGTGCCAGT	SYBR
ND5 (long, 930 bp amplicon)	F: CGCCTACTCCTCAGTTAGCC R: ATGGTGACTCAGTGCCAGGT	SYBR
ND2/ND1 (long, 832 bp amplicon)	F: GGATGAGCCTCAAACTCCAA R: ATGATGGCAAGGGTGATAGG	SYBR
D loop (short)	F: TGACTATCCCCTTCCCCATT R: TTGTTGGTTTCACGGAGGAT	SYBR
COII/ATPase 6 (short)	F: TCTCCCCTCTCTACGCATTC R: CGGTTAATACGGGGTTGTTG	SYBR
ND5 (short)	F: GGCCTCACATCATCACTCCT R: GCTGTGGATCCGTTCGTAGT	SYBR
ND2/ND1 (short)	F: GGATGAGCCTCAAACTCCAA R: GGCTCGTAAAGCTCCGAATA	SYBR
ACTINB	Mm00607939_s1	TaqMan

Human

Target	Sequence	Platform
HK-2	Hs00606086_m1	TaqMan
GLUT1	Hs00892681_m1	TaqMan
IL-1α	Hs00174092_m1	TaqMan
IL-1β	Hs01555410_m1	TaqMan
TNFα	Hs00174128_m1	TaqMan
IL-6	Hs00174131_m1	TaqMan
IL-10	Hs00961622_m1	TaqMan
MT-ATP-6	Hs02596862_g1	TaqMan
MT-CO2	Hs02596865_g1	TaqMan
ND1	F: CCATAAAACCCGCCACACT R: GAGCGATGGTGAGAGCTAAGGT	SYBR
18S	F: CGCAGCTAGGAATAATGGAATAGG R: CATGGCCTCAGTTCCGAAA	SYBR
CNX43	Hs.PT.58.38338544	SYBR
COX2	Hs.PT.58.77266	SYBR
ACTB	Hs.PT.39a.22214847	SYBR
YWHAZ	Hs01122445_g1	TaqMan

Table 3. Antibodies

Target	Species	Working Concentration	Source
Cox IV	Mouse IgG mAb	1:1,000	Cell Signaling Technology, #11967S
β-Actin-HRP	Rabbit IgG mAb	1:2,000	Cell Signaling Technology, #5125S
HIF1	Rabbit	1:1000	Cell Signaling Technology, #14179S

453 *RNA-Seq.* Following 6 days of treatment with CoCl2 100 μM versus control media, total RNA was
454 isolated from JAR cells as described above. Extracted RNA (300ng) was treated with NEBNext
455 rRNA Depletion Kit v2 (E7400X) and cDNA was generated using random hexamer priming and
456 Maxima H Minus Reverse Transcriptase. cDNA was converted into double stranded cDNA using
457 NEBNext mRNA Second Strand Synthesis Module (E6111L) and sequencing libraries were
458 generated by tagmentation using Nextera XT DNA Library Preparation Kit (Illumina FC-131) with
459 12 cycles of PCR amplification. Sequencing libraries were analyzed by Qubit and Agilent
460 Bioanalyzer, pooled at a final concentration of 1.2pM, and sequenced on an Illumina
461 Nextseq500 instrument 36x8x36 read structure.
462
463 *Transcriptomics Analysis*: Sequencing reads were demultiplexed and trimmed for adapters
464 using bcl2fastq (v2.20.0). Secondary adapter trimming, NextSeq/Poly(G) tail trimming, and read
465 filtering was performed using fastp (v0.20.0)[70]; low quality reads and reads shorter than 18nt
466 after trimming were removed from the read pool. Salmon (v1.1.0)[71] was used to simultaneously
467 map and quantify reads to transcripts in the GENCODE 33 genome annotation of the
468 GRCh38/hg38 human assembly. Salmon was run using full selective alignment, with sequence-
469 specific and fragment GC-bias correction turned on (--seqBias and --gcBias options,
470 respectively). Transcript abundances were collated and summarized to gene abundances using
471 the tximport package for R[72]. Normalization and differential expression analysis were
472 performed using edgeR[73,74]. For differential gene expression analysis, genes were considered
473 significant if they passed a fold change (FC) cutoff of log2FC > 1 and a false discovery rate (FDR)

474 cutoff of FDR < 0.05. Functional enrichment analyses were performed using g:Profiler[75].

475 WGCNA[76] was performed after removing genes with low expression as previously described[77].

476

477 *Statistics.* Student's two-tailed unpaired t-test, ordinary one-way, and two-way ANOVA

478 statistical tests were applied as indicated to compare biological replicates in each experiment.

479 Data were excluded as outliers using the interquartile range method (lower limit = 1st quartile –

480 1.5 x IQR; upper limit = 3rd quartile + 1.5 x IQR).

481

482 *Study Approval.* All animal experiments were approved by the Beth Israel Deaconess Medical

483 Center Institutional Animal Care and Use Committee (protocol #008-2022). Human placental

484 specimens and data were biobanked and accessed under protocols approved by the Beth Israel

485 Deaconess Medical Center Institutional Review Board, and written informed consent was

486 obtained before subject participation (protocols #2008P000061, 2020P000997, 2021P000897).

487

488 **Author Contributions:**

489 EJC, LT, SAK, and SMP designed the studies. HS, CJ, and LT performed WCGNA and JAR cell

490 transcriptomic assay and analyses. EJC and PF conducted *in vitro*, human placenta, and mouse

491 experiments and analyzed their results. EJC, SAK, and SMP wrote the manuscript with input

492 and approval from all authors.

493

494 **Acknowledgements:**

495 We thank Dr. Jennifer Condon of Wayne State University School of Medicine for generously

496 providing the hTERT-HM cell line.

We thank Saira Salahuddin for maintaining the placenta biorepository and helping access the study samples and accompanying clinical data.

Figures were created using Biorender.com.

Research reported in this publication was supported by the Institute of General Medical Sciences of the National Institutes of Health under award GM007592-41 and the Foundation for Anesthesia Education and Research (FAER) (EJC).

The authors declare no competing interests.

511 **References:**

512 1. Liu, L., Oza, S., Hogan, D., Perin, J., Rudan, I., Lawn, J.E., Cousens, S., Mathers, C., and
513 Black, R.E. (2015). Global, regional, and national causes of child mortality in 2000-13,
514 with projections to inform post-2015 priorities: an updated systematic analysis. Lancet
515 *385*, 430-440. 10.1016/S0140-6736(14)61698-6.

516 2. Blencowe, H., Cousens, S., Chou, D., Oestergaard, M., Say, L., Moller, A.B., Kinney, M.,
517 Lawn, J., and Born Too Soon Preterm Birth Action, G. (2013). Born too soon: the global
518 epidemiology of 15 million preterm births. Reprod Health *10 Suppl 1*, S2. 10.1186/1742-
519 4755-10-S1-S2.

520 3. Goldenberg, R.L., Culhane, J.F., Iams, J.D., and Romero, R. (2008). Epidemiology and
521 causes of preterm birth. Lancet *371*, 75-84. 10.1016/S0140-6736(08)60074-4.

522 4. Smith, V., Devane, D., Begley, C.M., Clarke, M., and Higgins, S. (2009). A systematic
523 review and quality assessment of systematic reviews of randomised trials of
524 interventions for preventing and treating preterm birth. Eur J Obstet Gynecol Reprod
525 Biol *142*, 3-11. 10.1016/j.ejogrb.2008.09.008.

526 5. Romero, R., Dey, S.K., and Fisher, S.J. (2014). Preterm labor: one syndrome, many
527 causes. Science *345*, 760-765. 10.1126/science.1251816.

528 6. Kiserud, T., Ebbing, C., Kessler, J., and Rasmussen, S. (2006). Fetal cardiac output,
529 distribution to the placenta and impact of placental compromise. Ultrasound Obstet
530 Gynecol *28*, 126-136. 10.1002/uog.2832.

531 7. Shaut, C.A., Keene, D.R., Sorensen, L.K., Li, D.Y., and Stadler, H.S. (2008). HOXA13 Is
532 essential for placental vascular patterning and labyrinth endothelial specification. PLoS
533 Genet *4*, e1000073. 10.1371/journal.pgen.1000073.
534 8. Lykke, J.A., Langhoff-Roos, J., Sibai, B.M., Funai, E.F., Triche, E.W., and Paidas, M.J.
535 (2009). Hypertensive pregnancy disorders and subsequent cardiovascular morbidity and
536 type 2 diabetes mellitus in the mother. Hypertension *53*, 944-951.
537 10.1161/HYPERTENSIONAHA.109.130765.
538 9. Genbacev, O., Joslin, R., Damsky, C.H., Polliotti, B.M., and Fisher, S.J. (1996). Hypoxia
539 alters early gestation human cytotrophoblast differentiation/invasion in vitro and
540 models the placental defects that occur in preeclampsia. J Clin Invest *97*, 540-550.
541 10.1172/JCI118447.
542 10. Plaks, V., Rinkenberger, J., Dai, J., Flannery, M., Sund, M., Kanasaki, K., Ni, W., Kalluri, R.,
543 and Werb, Z. (2013). Matrix metalloproteinase-9 deficiency phenocopies features of
544 preeclampsia and intrauterine growth restriction. Proc Natl Acad Sci U S A *110*, 11109-
545 11114. 10.1073/pnas.1309561110.
546 11. Li, F., Fushima, T., Oyanagi, G., Townley-Tilson, H.W., Sato, E., Nakada, H., Oe, Y.,
547 Hagaman, J.R., Wilder, J., Li, M., et al. (2016). Nicotinamide benefits both mothers and
548 pups in two contrasting mouse models of preeclampsia. Proc Natl Acad Sci U S A *113*,
549 13450-13455. 10.1073/pnas.1614947113.
550 12. Romero, R., and Chaiworapongsa, T. (2013). Preeclampsia: a link between trophoblast
551 dysregulation and an antiangiogenic state. J Clin Invest *123*, 2775-2777.
552 10.1172/JCI70431.

553 13. McIntyre, K.R., Vincent, K.M.M., Hayward, C.E., Li, X., Sibley, C.P., Desforges, M.,
554 Greenwood, S.L., and Dilworth, M.R. (2020). Human placental uptake of glutamine and
555 glutamate is reduced in fetal growth restriction. Sci Rep *10*, 16197. 10.1038/s41598-
556 020-72930-7.
557 14. Xu, Y.Y., Liu, Y., Cui, L., Wu, W.B., Quinn, M.J., Menon, R., and Zhang, H.J. (2021).
558 Hypoxic effects on the mitochondrial content and functions of the placenta in fetal
559 growth restriction. Placenta *114*, 100-107. 10.1016/j.placenta.2021.09.003.
560 15. Koga, K., Cardenas, I., Aldo, P., Abrahams, V.M., Peng, B., Fill, S., Romero, R., and Mor, G.
561 (2009). Activation of TLR3 in the trophoblast is associated with preterm delivery. Am J
562 Reprod Immunol *61*, 196-212. 10.1111/j.1600-0897.2008.00682.x.
563 16. Pique-Regi, R., Romero, R., Tarca, A.L., Sendler, E.D., Xu, Y., Garcia-Flores, V., Leng, Y.,
564 Luca, F., Hassan, S.S., and Gomez-Lopez, N. (2019). Single cell transcriptional signatures
565 of the human placenta in term and preterm parturition. Elife *8*. 10.7554/eLife.52004.
566 17. Beharier, O., Tyurin, V.A., Goff, J.P., Guerrero-Santoro, J., Kajiwara, K., Chu, T., Tyurina,
567 Y.Y., St Croix, C.M., Wallace, C.T., Parry, S., et al. (2020). PLA2G6 guards placental
568 trophoblasts against ferroptotic injury. Proc Natl Acad Sci U S A *117*, 27319-27328.
569 10.1073/pnas.2009201117.
570 18. Elshenawy, S., Pinney, S.E., Stuart, T., Doulias, P.T., Zura, G., Parry, S., Elovitz, M.A.,
571 Bennett, M.J., Bansal, A., Strauss, J.F., 3rd, et al. (2020). The Metabolomic Signature of
572 the Placenta in Spontaneous Preterm Birth. Int J Mol Sci *21*. 10.3390/ijms21031043.
573 19. Lien, Y.C., Zhang, Z., Cheng, Y., Polyak, E., Sillers, L., Falk, M.J., Ischiropoulos, H., Parry, S.,
574 and Simmons, R.A. (2021). Human Placental Transcriptome Reveals Critical Alterations in

575 Inflammation and Energy Metabolism with Fetal Sex Differences in Spontaneous
576 Preterm Birth. Int J Mol Sci *22*. 10.3390/ijms22157899.
577 20. Paquette, A.G., Brockway, H.M., Price, N.D., and Muglia, L.J. (2018). Comparative
578 transcriptomic analysis of human placentae at term and preterm delivery. Biol Reprod
579 *98*, 89-101. 10.1093/biolre/iox163.
580 21. Edgar, R., Domrachev, M., and Lash, A.E. (2002). Gene Expression Omnibus: NCBI gene
581 expression and hybridization array data repository. Nucleic Acids Res *30*, 207-210.
582 10.1093/nar/30.1.207.
583 22. Knox, K., and Baker, J.C. (2008). Genomic evolution of the placenta using co-option and
584 duplication and divergence. Genome Res *18*, 695-705. 10.1101/gr.071407.107.
585 23. Zhou, Q.Y., Fang, M.D., Huang, T.H., Li, C.C., Yu, M., and Zhao, S.H. (2009). Detection of
586 differentially expressed genes between Erhualian and Large White placentas on day 75
587 and 90 of gestation. BMC Genomics *10*, 337. 10.1186/1471-2164-10-337.
588 24. Loux, S.C., Dini, P., El-Sheikh Ali, H., Kalbfleisch, T., and Ball, B.A. (2019). Characterization
589 of the placental transcriptome through mid to late gestation in the mare. PLoS One *14*,
590 e0224497. 10.1371/journal.pone.0224497.
591 25. Soncin, F., Khater, M., To, C., Pizzo, D., Farah, O., Wakeland, A., Arul Nambi Rajan, K.,
592 Nelson, K.K., Chang, C.W., Moretto-Zita, M., et al. (2018). Comparative analysis of
593 mouse and human placentae across gestation reveals species-specific regulators of
594 placental development. Development *145*. 10.1242/dev.156273.
595 26. Maeda, K.J., Showmaker, K.C., Johnson, A.C., Garrett, M.R., and Sasser, J.M. (2019).
596 Spontaneous superimposed preeclampsia: chronology and expression unveiled by

597 temporal transcriptomic analysis. Physiol Genomics *51*, 342-355.
598 10.1152/physiolgenomics.00020.2019.
599 27. Morey, R., Farah, O., Kallol, S., Requena, D.F., Meads, M., Moretto-Zita, M., Soncin, F.,
600 Laurent, L.C., and Parast, M.M. (2021). Transcriptomic Drivers of Differentiation,
601 Maturation, and Polyploidy in Human Extravillous Trophoblast. Front Cell Dev Biol *9*,
602 702046. 10.3389/fcell.2021.702046.
603 28. Steinhauser, C.B., Lambo, C.A., Askelson, K., Burns, G.W., Behura, S.K., Spencer, T.E.,
604 Bazer, F.W., and Satterfield, M.C. (2021). Placental Transcriptome Adaptations to
605 Maternal Nutrient Restriction in Sheep. Int J Mol Sci *22*. 10.3390/ijms22147654.
606 29. Lee, B.Y., Han, J.A., Im, J.S., Morrone, A., Johung, K., Goodwin, E.C., Kleijer, W.J., DiMaio,
607 D., and Hwang, E.S. (2006). Senescence-associated beta-galactosidase is lysosomal beta-
608 galactosidase. Aging Cell *5*, 187-195. 10.1111/j.1474-9726.2006.00199.x.
609 30. Jang, J.Y., Blum, A., Liu, J., and Finkel, T. (2018). The role of mitochondria in aging. J Clin
610 Invest *128*, 3662-3670. 10.1172/JCI120842.
611 31. Trifunovic, A., Wredenberg, A., Falkenberg, M., Spelbrink, J.N., Rovio, A.T., Bruder, C.E.,
612 Bohlooly, Y.M., Gidlof, S., Oldfors, A., Wibom, R., et al. (2004). Premature ageing in mice
613 expressing defective mitochondrial DNA polymerase. Nature *429*, 417-423.
614 10.1038/nature02517.
615 32. Rothfuss, O., Gasser, T., and Patenge, N. (2010). Analysis of differential DNA damage in
616 the mitochondrial genome employing a semi-long run real-time PCR approach. Nucleic
617 Acids Res *38*, e24. 10.1093/nar/gkp1082.

618 33. Bratic, A., and Larsson, N.G. (2013). The role of mitochondria in aging. J Clin Invest *123*,
619 951-957. 10.1172/JCI64125.
620 34. Wiley, C.D., and Campisi, J. (2016). From Ancient Pathways to Aging Cells-Connecting
621 Metabolism and Cellular Senescence. Cell Metab *23*, 1013-1021.
622 10.1016/j.cmet.2016.05.010.
623 35. Wiley, C.D., and Campisi, J. (2021). The metabolic roots of senescence: mechanisms and
624 opportunities for intervention. Nat Metab *3*, 1290-1301. 10.1038/s42255-021-00483-8.
625 36. Maxwell, P.H., Wiesener, M.S., Chang, G.W., Clifford, S.C., Vaux, E.C., Cockman, M.E.,
626 Wykoff, C.C., Pugh, C.W., Maher, E.R., and Ratcliffe, P.J. (1999). The tumour suppressor
627 protein VHL targets hypoxia-inducible factors for oxygen-dependent proteolysis. Nature
628 *399*, 271-275. 10.1038/20459.
629 37. Jaakkola, P., Mole, D.R., Tian, Y.M., Wilson, M.I., Gielbert, J., Gaskell, S.J., von
630 Kriegsheim, A., Hebestreit, H.F., Mukherji, M., Schofield, C.J., et al. (2001). Targeting of
631 HIF-alpha to the von Hippel-Lindau ubiquitylation complex by O2-regulated prolyl
632 hydroxylation. Science *292*, 468-472. 10.1126/science.1059796.
633 38. Nursalim, Y.N.S., Blenkiron, C., Groom, K.M., and Chamley, L.W. (2020). Growing human
634 trophoblasts in vitro: a review of the media commonly used in trophoblast cell culture.
635 Reproduction *160*, R119-R128. 10.1530/REP-19-0605.
636 39. Rothbauer, M., Patel, N., Gondola, H., Siwetz, M., Huppertz, B., and Ertl, P. (2017). A
637 comparative study of five physiological key parameters between four different human
638 trophoblast-derived cell lines. Sci Rep *7*, 5892. 10.1038/s41598-017-06364-z.

639 40. Epstein, A.C., Gleadle, J.M., McNeill, L.A., Hewitson, K.S., O'Rourke, J., Mole, D.R.,
640 Mukherji, M., Metzen, E., Wilson, M.I., Dhanda, A., et al. (2001). C. elegans EGL-9 and
641 mammalian homologs define a family of dioxygenases that regulate HIF by prolyl
642 hydroxylation. Cell *107*, 43-54. 10.1016/s0092-8674(01)00507-4.
643 41. Nishimura, F., Mogami, H., Moriuchi, K., Chigusa, Y., Mandai, M., and Kondoh, E. (2020).
644 Mechanisms of thrombin-Induced myometrial contractions: Potential targets of
645 progesterone. PLoS One *15*, e0231944. 10.1371/journal.pone.0231944.
646 42. Rauk, P.N., and Chiao, J.P. (2000). Interleukin-1 stimulates human uterine prostaglandin
647 production through induction of cyclooxygenase-2 expression. Am J Reprod Immunol
648 *43*, 152-159. 10.1111/j.8755-8920.2000.430304.x.
649 43. Leimert, K.B., Verstraeten, B.S.E., Messer, A., Nemati, R., Blackadar, K., Fang, X.,
650 Robertson, S.A., Chemtob, S., and Olson, D.M. (2019). Cooperative effects of sequential
651 PGF2alpha and IL-1beta on IL-6 and COX-2 expression in human myometrial cellsdagger.
652 Biol Reprod *100*, 1370-1385. 10.1093/biolre/ioz029.
653 44. Devost, D., and Zingg, H.H. (2007). Novel in vitro system for functional assessment of
654 oxytocin action. Am J Physiol Endocrinol Metab *292*, E1-6.
655 10.1152/ajpendo.00529.2005.
656 45. Campisi, J., Kapahi, P., Lithgow, G.J., Melov, S., Newman, J.C., and Verdin, E. (2019).
657 From discoveries in ageing research to therapeutics for healthy ageing. Nature *571*, 183-
658 192. 10.1038/s41586-019-1365-2.
659 46. Rosso, P. (1976). Placenta as an aging organ. Curr Concepts Nutr *4*, 23-41.

660 47. Martin, B.J., and Spicer, S.S. (1973). Ultrastructural features of cellular maturation and
661 aging in human trophoblast. J Ultrastruct Res *43*, 133-149. 10.1016/s0022-
662 5320(73)90074-9.
663 48. Fox, H. (1997). Aging of the placenta. Arch Dis Child Fetal Neonatal Ed *77*, F171-175.
664 10.1136/fn.77.3.f171.
665 49. Sultana, Z., Maiti, K., Aitken, J., Morris, J., Dedman, L., and Smith, R. (2017). Oxidative
666 stress, placental ageing-related pathologies and adverse pregnancy outcomes. Am J
667 Reprod Immunol *77*. 10.1111/aji.12653.
668 50. Cindrova-Davies, T., Fogarty, N.M.E., Jones, C.J.P., Kingdom, J., and Burton, G.J. (2018).
669 Evidence of oxidative stress-induced senescence in mature, post-mature and
670 pathological human placentas. Placenta *68*, 15-22. 10.1016/j.placenta.2018.06.307.
671 51. Biron-Shental, T., Sukenik-Halevy, R., Sharon, Y., Goldberg-Bittman, L., Kidron, D., Fejgin,
672 M.D., and Amiel, A. (2010). Short telomeres may play a role in placental dysfunction in
673 preeclampsia and intrauterine growth restriction. Am J Obstet Gynecol *202*, 381 e381-
674 387. 10.1016/j.ajog.2010.01.036.
675 52. Chen, K.H., Chen, L.R., and Lee, Y.H. (2011). Exploring the relationship between preterm
676 placental calcification and adverse maternal and fetal outcome. Ultrasound Obstet
677 Gynecol *37*, 328-334. 10.1002/uog.7733.
678 53. Maiti, K., Sultana, Z., Aitken, R.J., Morris, J., Park, F., Andrew, B., Riley, S.C., and Smith, R.
679 (2017). Evidence that fetal death is associated with placental aging. Am J Obstet Gynecol
680 *217*, 441 e441-441 e414. 10.1016/j.ajog.2017.06.015.

681 54. Bonney, E.A., Krebs, K., Saade, G., Kechichian, T., Trivedi, J., Huaizhi, Y., and Menon, R.
682 (2016). Differential senescence in feto-maternal tissues during mouse pregnancy.
683 Placenta *43*, 26-34. 10.1016/j.placenta.2016.04.018.
684 55. Menon, R., Behnia, F., Polettini, J., Saade, G.R., Campisi, J., and Velarde, M. (2016).
685 Placental membrane aging and HMGB1 signaling associated with human parturition.
686 Aging (Albany NY) *8*, 216-230. 10.18632/aging.100891.
687 56. Menon, R., Richardson, L.S., and Lappas, M. (2019). Fetal membrane architecture, aging
688 and inflammation in pregnancy and parturition. Placenta *79*, 40-45.
689 10.1016/j.placenta.2018.11.003.
690 57. Hirota, Y., Daikoku, T., Tranguch, S., Xie, H., Bradshaw, H.B., and Dey, S.K. (2010).
691 Uterine-specific p53 deficiency confers premature uterine senescence and promotes
692 preterm birth in mice. J Clin Invest *120*, 803-815. 10.1172/JCI40051.
693 58. Hirota, Y., Cha, J., Yoshie, M., Daikoku, T., and Dey, S.K. (2011). Heightened uterine
694 mammalian target of rapamycin complex 1 (mTORC1) signaling provokes preterm birth
695 in mice. Proc Natl Acad Sci U S A *108*, 18073-18078. 10.1073/pnas.1108180108.
696 59. Nye, G.A., Ingram, E., Johnstone, E.D., Jensen, O.E., Schneider, H., Lewis, R.M.,
697 Chernyavsky, I.L., and Brownbill, P. (2018). Human placental oxygenation in late
698 gestation: experimental and theoretical approaches. J Physiol *596*, 5523-5534.
699 10.1113/JP275633.
700 60. Gomes, A.P., Price, N.L., Ling, A.J., Moslehi, J.J., Montgomery, M.K., Rajman, L., White,
701 J.P., Teodoro, J.S., Wrann, C.D., Hubbard, B.P., et al. (2013). Declining NAD(+) induces a

702 pseudohypoxic state disrupting nuclear-mitochondrial communication during aging. Cell
703 *155*, 1624-1638. 10.1016/j.cell.2013.11.037.
704 61. Gonzalez, T.L., Eisman, L.E., Joshi, N.V., Flowers, A.E., Wu, D., Wang, Y., Santiskulvong,
705 C., Tang, J., Buttle, R.A., Sauro, E., et al. (2021). High-throughput miRNA sequencing of
706 the human placenta: expression throughout gestation. Epigenomics *13*, 995-1012.
707 10.2217/epi-2021-0055.
708 62. Sferruzzi-Perri, A.N., Higgins, J.S., Vaughan, O.R., Murray, A.J., and Fowden, A.L. (2019).
709 Placental mitochondria adapt developmentally and in response to hypoxia to support
710 fetal growth. Proc Natl Acad Sci U S A *116*, 1621-1626. 10.1073/pnas.1816056116.
711 63. Albers, R.E., Kaufman, M.R., Natale, B.V., Keoni, C., Kulkarni-Datar, K., Min, S., Williams,
712 C.R., Natale, D.R.C., and Brown, T.L. (2019). Trophoblast-Specific Expression of Hif-
713 1alpha Results in Preeclampsia-Like Symptoms and Fetal Growth Restriction. Sci Rep *9*,
714 2742. 10.1038/s41598-019-39426-5.
715 64. Rasmussen, S., Ebbing, C., and Irgens, L.M. (2017). Predicting preeclampsia from a
716 history of preterm birth. PLoS One *12*, e0181016. 10.1371/journal.pone.0181016.
717 65. Mando, C., De Palma, C., Stampalija, T., Anelli, G.M., Figus, M., Novielli, C., Parisi, F.,
718 Clementi, E., Ferrazzi, E., and Cetin, I. (2014). Placental mitochondrial content and
719 function in intrauterine growth restriction and preeclampsia. Am J Physiol Endocrinol
720 Metab *306*, E404-413. 10.1152/ajpendo.00426.2013.
721 66. Fujimaki, A., Watanabe, K., Mori, T., Kimura, C., Shinohara, K., and Wakatsuki, A. (2011).
722 Placental oxidative DNA damage and its repair in preeclamptic women with fetal growth
723 restriction. Placenta *32*, 367-372. 10.1016/j.placenta.2011.02.004.

724 67. Davy, P., Nagata, M., Bullard, P., Fogelson, N.S., and Allsopp, R. (2009). Fetal growth
725 restriction is associated with accelerated telomere shortening and increased expression
726 of cell senescence markers in the placenta. Placenta *30*, 539-542.
727 10.1016/j.placenta.2009.03.005.
728 68. Burton, G.J., Yung, H.W., Cindrova-Davies, T., and Charnock-Jones, D.S. (2009). Placental
729 endoplasmic reticulum stress and oxidative stress in the pathophysiology of unexplained
730 intrauterine growth restriction and early onset preeclampsia. Placenta *30 Suppl A*, S43-
731 48. 10.1016/j.placenta.2008.11.003.
732 69. Pennington, K.A., Schlitt, J.M., and Schulz, L.C. (2012). Isolation of primary mouse
733 trophoblast cells and trophoblast invasion assay. J Vis Exp, e3202. 10.3791/3202.
734 70. Chen, S., Zhou, Y., Chen, Y., and Gu, J. (2018). fastp: an ultra-fast all-in-one FASTQ
735 preprocessor. Bioinformatics *34*, i884-i890. 10.1093/bioinformatics/bty560.
736 71. Patro, R., Duggal, G., Love, M.I., Irizarry, R.A., and Kingsford, C. (2017). Salmon provides
737 fast and bias-aware quantification of transcript expression. Nat Methods *14*, 417-419.
738 10.1038/nmeth.4197.
739 72. Soneson, C., Love, M.I., and Robinson, M.D. (2015). Differential analyses for RNA-seq:
740 transcript-level estimates improve gene-level inferences. F1000Res *4*, 1521.
741 10.12688/f1000research.7563.2.
742 73. Robinson, M.D., McCarthy, D.J., and Smyth, G.K. (2010). edgeR: a Bioconductor package
743 for differential expression analysis of digital gene expression data. Bioinformatics *26*,
744 139-140. 10.1093/bioinformatics/btp616.

745 74. Chen, Y., Lun, A.T., and Smyth, G.K. (2016). From reads to genes to pathways:
746 differential expression analysis of RNA-Seq experiments using Rsubread and the edgeR
747 quasi-likelihood pipeline. F1000Res *5*, 1438. 10.12688/f1000research.8987.2.
748 75. Raudvere, U., Kolberg, L., Kuzmin, I., Arak, T., Adler, P., Peterson, H., and Vilo, J. (2019).
749 g:Profiler: a web server for functional enrichment analysis and conversions of gene lists
750 (2019 update). Nucleic Acids Res *47*, W191-W198. 10.1093/nar/gkz369.
751 76. Langfelder, P., and Horvath, S. (2008). WGCNA: an R package for weighted correlation
752 network analysis. BMC Bioinformatics *9*, 559. 10.1186/1471-2105-9-559.
753 77. Bentsen, M.A., Rausch, D.M., Mirzadeh, Z., Muta, K., Scarlett, J.M., Brown, J.M.,
754 Herranz-Perez, V., Baquero, A.F., Thompson, J., Alonge, K.M., et al. (2020).
755 Transcriptomic analysis links diverse hypothalamic cell types to fibroblast growth factor
756 1-induced sustained diabetes remission. Nat Commun *11*, 4458. 10.1038/s41467-020-
757 17720-5.
758